The most luminous, merger-free AGN show only marginal correlation with bar presence

Izzy L. Garland,[1]* Matthew J. Fahey,[1] Brooke D. Simmons,[1] Rebecca J. Smethurst,[2] Chris J. Lintott,[2] Jesse Shanahan,[3] Maddie S. Silcock,[1,4] Joshua Smith,[1] William C. Keel,[5] Alison Coil,[3] Tobias Géron,[2] Sandor Kruk,[6] Karen L. Masters,[7] David O'Ryan,[1] Matthew R. Thorne,[1] Klaas Wiersema[1]

[1]*Physics Department, Lancaster University, Lancaster, LA1 4YB, UK*
[2]*Oxford Astrophysics, Department of Physics, University of Oxford, Denys Wilkinson Building, Keble Road, Oxford, OX1 3RH, UK*
[3]*Center for Astrophysics and Space Sciences (CASS), Department of Physics, University of California, San Diego, CA 92093, USA*
[4]*Centre for Astrophysics Research, University of Hertfordshire, College Lane, Hatfield AL10 9AB, UK*
[5]*Department of Physics and Astronomy, University of Alabama, Box 870324, Tuscaloosa, AL 35404, USA*
[6]*Max-Planck-Institut für extraterrestrische Physik (MPE), Giessenbachstrasse 1, 85748 Garching bei München, Germany*
[7]*Haverford College, 370 Lancaster Avenue, Haverford, PA 19041, USA*

ABSTRACT

The role of large-scale bars in the fuelling of active galactic nuclei (AGN) is still debated, even as evidence mounts that black hole growth in the absence of galaxy mergers cumulatively dominates and may substantially influence disc (i.e., merger-free) galaxy evolution. We investigate whether large-scale galactic bars are a good candidate for merger-free AGN fuelling. Specifically, we combine slit spectroscopy and *Hubble Space Telescope* imagery to characterise star formation rates (SFRs) and stellar masses of the unambiguously disc-dominated host galaxies of a sample of luminous, Type-1 AGN with $0.02 < z < 0.24$. After carefully correcting for AGN signal, we find no clear difference in SFR between AGN hosts and a stellar mass-matched sample of galaxies lacking an AGN ($0.013 < z < 0.19$), although this could be due to small sample size ($n_{\rm AGN} = 34$). We correct for SFR and stellar mass to minimise selection biases, and compare the bar fraction in the two samples. We find that AGN are marginally ($\sim 1.7\sigma$) more likely to host a bar than inactive galaxies, with AGN hosts having a bar fraction, $f_{\rm bar} = 0.59^{+0.08}_{-0.09}$ and inactive galaxies having a bar fraction, $f_{\rm bar} = 0.44^{+0.08}_{-0.09}$. However, we find no further differences between SFR- and mass-matched AGN and inactive samples. While bars *could* potentially trigger AGN activity, they appear to have no further, unique effect on a galaxy's stellar mass or SFR.

Key words: galaxies: disc – galaxies: active – galaxies: bar – galaxies: star formation

1 INTRODUCTION

There are still many fundamental open questions about the interplay between galaxies and the supermassive black holes (SMBHs) they host. For example, whilst major galaxy mergers were thought to dominate black hole-galaxy co-evolution in previous decades (e.g., Kormendy & Ho 2013), more recent results have made clear that merger-free (sometimes called 'secular') processes are at least as important to the overall growth and evolution of black holes and galaxies as mergers, with their black hole-galaxy properties showing the same correlations as those undergoing merger-driven growth (e.g., Simmons et al. 2017), as described in more detail below.

From the theoretical perspective, multiple cosmological simulations find that a dominant majority of black hole growth occurs as a result of merger-free processes (at least 65 per cent, possibly more than 85 per cent, depending on the simulation; Martin et al. 2018; McAlpine et al. 2020). Observational works have long been accumulating evidence for the merger-free black hole growth pathway

(Greene et al. 2010; Jiang et al. 2011; Cisternas et al. 2011; Schawinski et al. 2011; Kocevski et al. 2012; Simmons et al. 2011, 2012, 2013; Smethurst et al. 2021), where often merger-free growth is isolated via the study of strongly disc-dominated galaxies (which have not had a significant merger since $z \sim 2$; Martig et al. 2012).

Given the diversity of evidence for substantial merger-free black hole growth at a range of redshifts, there must be a significant mechanism of fuelling AGN in the absence of major mergers. In these secularly built, disc-dominated galaxies, gas must still be transported to the central regions in order for an AGN to be present. Smethurst et al. (2019) calculate the necessary inflow rate (i.e. the minimum gas mass that must be provided by any means to the central SMBH) for their sample of AGN in disc-dominated galaxies, and show that bars (Shlosman et al. 1989, 1990; Knapen et al. 1995; Sakamoto et al. 1999; Maciejewski et al. 2002; Regan & Teuben 2004; Lin et al. 2013), spiral arms (Maciejewski 2004; Davies et al. 2009; Schnorr-Müller et al. 2014), and the smooth accretion of cold gas (Kereš et al. 2005; Sancisi et al. 2008) can each match the inflow rate required to sustain an AGN. These are all morphological features with a long lifespan (Miller & Smith 1979; Sparke & Sellwood 1987; Donner &

Thomasson 1994; D'Onghia et al. 2013; Hunt et al. 2018), orders of magnitude longer than the $\sim 10^5$ yr phases within the lifetime of an AGN (Schawinski et al. 2015), so if these features are able to periodically feed the SMBH (Schawinski et al. 2015) over their lifetimes, then the mass of the SMBH can grow to the masses observed in the present. In other words, the secular, calm processes seen in disc-dominated galaxies are more than capable of fuelling AGN (Smethurst et al. 2019).

Large-scale galactic bars, in particular, are a common feature in the local Universe, with Masters et al. (2011) estimating that around 29.4 ± 0.5 per cent of disc galaxies at redshift $0.01 < z < 0.06$ host a large-scale, strong galactic bar when observed in optical wavelengths. Barazza et al. (2008) examine bar fraction in the *r*-band specifically, and report a bar fraction of 48 per cent to 52 per cent, however in infra-red imaging, a bar fraction as high as 70 per cent has been observed (Mulchaey & Regan 1997; Knapen et al. 2000; Eskridge et al. 2000). Theoretical studies of AGN fuelling in disc galaxies show that bars are a viable method of transporting matter to a central SMBH (Friedli & Benz 1993; Athanassoula 1992, 2003; Ann & Thakur 2005).

Despite bars being relatively common in disc galaxies and theoretically able to power a luminous AGN, observing such a connection has proven difficult. Many studies find no correlation between bars and AGN (Martini et al. 2003; Oh et al. 2012; Lee et al. 2012; Cheung et al. 2015; Goulding et al. 2017), whereas studies such as Knapen et al. (2000), Laine et al. (2002), and Laurikainen et al. (2004) show there is an increase in the number of AGN host galaxies containing bars of around 20 per cent. Galloway et al. (2015) note that there is a higher probability of an AGN host galaxy possessing a strong bar than a galaxy without an AGN, but find no link between bars and the quantity or efficiency of AGN fuelling, indicating that whilst the presence of a strong bar may trigger the "turn on" of the AGN, the bar then drives accretion in a way that is indistinguishable from the secular processes that would be fuelling the AGN in the bar's absence.

Several factors likely contribute to the difficulty of observing a connection between AGN and bars. AGN are more likely to reside in galaxies with a higher stellar mass, M_* (Kauffmann et al. 2003b; Aird et al. 2012), and a correlation between bars and stellar mass has been observed, although the nature of this correlation is debated, potentially with bars being more likely to reside in galaxies with a higher stellar mass (e.g. Skibba et al. 2012), although a study conducted in Erwin (2018) highlights that this may be a selection effect, and shows that bar presence may peak at $\log(M_*/M_\odot) = 9.7$ and decrease either side of this value. Bars are also more likely to reside in redder galaxies (i.e., less star-forming) (Masters et al. 2011, 2012; Skibba et al. 2012; Oh et al. 2012; Cheung et al. 2013; Kruk et al. 2018; Géron et al. 2021), but in some cases, enhancement of star formation rate (SFR) in a circumnuclear ring at the centre has been observed (Hawarden et al. 1986). Controlling for these confounding variables in order to understand how bars, star formation, and black hole growth may affect each other requires large samples and careful measurements.

There is another crucial caveat in determining any link between bars and AGN which causes significant problems: both features have drastically different typical lifetimes. SMBH tend to only be in the AGN phase for around 10^5 yr (Schawinski et al. 2015), whereas bars are long-lived features (Sellwood 2014), with simulations showing bars that form at $z \sim 1.3$ can maintain their strength down to $z \sim 0$ (Kraljic et al. 2012). This corresponds to a lookback time of 8.9Gyr, meaning that bars can live at least 100,000 times as long as an AGN phase. This means that when a barred galaxy is observed, we may not observe AGN activity because the AGN has since faded. Since bars tend to facilitate the development of pseudobulges over time via the buckling of stellar orbits (see Combes 2009 for a review), observing galaxies with no or very small bulges may aid in mitigating this issue, as then any bars observed would be younger, and have less chance of outliving an AGN at the time of observation.

There is also very little consensus on the link between AGN and SFR (e.g. Mulcahey et al. 2022). Additionally, it is a challenge to measure SFRs in galaxies hosting luminous AGN. Star formation and AGN appear to share a common fuel source (Silverman et al. 2009); thus if there is more of this fuel source, we would expect to see an increase in AGN and in SFR appearing together. This has been observed (e.g. Mullaney et al. 2012; Aird et al. 2019). However, AGN feedback has also been shown to be capable of affecting the star formation in the host galaxy. For example, positive feedback can occur when an outflow compresses the molecular clouds or the interstellar medium in its path, thus increasing SFR (Ishibashi & Fabian 2012; Schaye et al. 2015). Negative feedback can quench star formation via heating the molecular gas and interstellar medium (e.g. Ciotti et al. 2010). See Fabian (2012) for a review on AGN feedback and star formation.
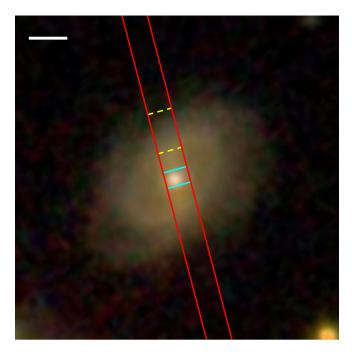
In this work, we examine AGN in unambiguously disc-dominated ('bulgeless') galaxies in order to isolate SMBH growth in the merger-free regime. As mentioned above, these disc-dominated galaxies indicate a merger-free history since at least $z \sim 2$, due to mergers resulting in a central bulge (Martig et al. 2012). Previous studies have shown that these AGN exist at a range of black hole masses and luminosities, (Satyapal et al. 2009; Simmons et al. 2013; Bizzocchi et al. 2014; Satyapal et al. 2016). Simmons, Smethurst & Lintott (2017) compiled a sample of relatively nearby ($z < 0.25$) unobscured, luminous AGN residing in disc-dominated systems. Despite having long-term evolutionary histories free of significant mergers, these systems lie on SMBH–galaxy co-evolution relations which were originally observed in elliptical galaxies with a history of major mergers (Häring & Rix 2004). This unique sample of merger-free quasars is the parent sample for the data used in this work. There has not yet been a detailed study of bars and AGN in these systems in the same way that there has been in the general galaxy population.

We use spectra taken from the Shane Telescope at Lick Observatory to examine the SFRs in merger-free galaxies hosting luminous AGN. We also investigate whether, after controlling for parameters such as SFR and M_*, a correlation can be observed between the presence of a bar and the presence of an AGN. We discuss data collection, comparison samples and fitting procedures in Section 2, and we determine stellar properties of our sample in Section 3. We discuss SFR in Section 4, and then examine the bar fractions in Section 5, before concluding in Section 6.

Throughout this paper, the term 'active galaxy' refers to a galaxy that hosts an AGN, and the term 'inactive galaxy' refers to a galaxy that does not host an AGN. These two terms do not refer to the star formation in the galaxy. We use WMAP9 cosmology (Hinshaw et al. 2013), where we assume a flat universe, $H_0 = 69.3 \, \mathrm{km \, s^{-1} \, Mpc^{-1}}$ and $\Omega_m = 0.287$.

2 SAMPLE AND OBSERVATIONS

This study uses multiple samples and data sources. In the subsections below, we describe our main sample of AGN host galaxies, as well as our comparison sample of inactive disc galaxies. We further describe the data reduction, spectral fitting, and morphological fitting procedures used for each of these samples.

have neither SDSS fibre spectra nor Lick longslit spectra. 21 of the sources have both longslit and fibre spectra. Throughout this work, this sample of 56 sources shall be referred to as AɢɴDɪsᴄs, and SDSS images of these sources are shown in Appendix A.

2.2 Inactive Sample

In order to investigate bar-driven fuelling of AGN, it is necessary to compare the AGN host sample to a resolution-matched and morphology-matched sample of galaxies which lack AGN activity signatures but are otherwise similar. This allows us to separate out any properties that may appear to be a result of bar presence, but are actually a result of AGN presence, as well as provide a baseline comparison for how a bar can affect a galaxy in the absence of an AGN. Typically, when selecting comparison samples, stellar mass is also matched, and whilst we do perform this matching later on in Section 4, we first want to see how the stellar mass (along with the star formation rate) varies between AɢɴDɪsᴄs and the inactive galaxies.

We used Galaxy Zoo 2 (GZ2; Willett et al. 2013) to first identify a sample of disc-dominated galaxies. Volunteers are shown an image from SDSS, and asked via the question tree shown in Willett et al. (2013) to classify the central galaxy in the image. The first question asked is 'Is the galaxy smooth and rounded, with no sign of a disc?', and for this work, we require that the vote fraction for those who answered that the galaxy is featured be $p_{features\,or\,disc} \geq 0.35$, following the suggestion in Galloway et al. (2015) based on expert visual inspection. This leads the volunteers who answered 'No' (i.e. the galaxy is featured) to the question 'Could this be a disc viewed edge on?'. We require a sample of face-on discs so that we can identify a bar if one is present. In an edge-on disc, the bar is often hidden by the geometry of the galaxy. We require that the vote fraction of volunteers classing the disc as not-edge-on be $p_{not\,edge\,on} \geq 0.6$, again following the suggestion in Galloway et al. (2015). This makes up our inactive disc sample.

To establish the lack of AGN, we use the fluxes from OSSY (Oh et al. 2011) to divide the sample into AGN hosts, star-forming galaxies, composite sources, and LINERs. To build the inactive sample, we exclusively use sources that fall into the star-forming category. This is to ensure purity of the sample. We exclude any source where the emission lines [O III], [N II], Hα, and Hα have a signal–to–noise ratio, $S/N < 3$. We use the guidance in Kauffmann et al. (2003b, Equation 1), where they show that a source is star-forming if

$$\log\left([\text{O\,III}]\lambda6584/\text{H}\beta\right) < \frac{0.61}{\log\left([\text{N\,II}]\lambda6584/\text{H}\alpha\right) - 0.05} + 1.3 \quad (1)$$

We impose a limit on the resolution rather than the redshift, since the bars are identified visually. We need to ensure the resolution distribution of active galaxies covers the same range as our sample of inactive galaxies. This is particularly important given that the inactive galaxies have their bar presence determined through SDSS images (via GZ2 volunteers), but only around half of the active galaxies use SDSS for bar identification - the rest use *HST* images, which have a far better resolution and thus can push to higher redshift before the classification of bar presence is marred by significant doubt - see Section 2.4 for a more detailed description of identifying bars. For AGN hosts with *HST* images, we determine what their equivalent redshift would be if they were observed solely with SDSS to obtain the same resolution in arcseconds per pixel. We use these equivalent redshifts to determine that the maximum redshift of our inactive sample should be $z > 0.187$. Ensuring this resolution matching

Figure 1. SDSS postage stamp of J081324.00+542236.9, overlain with the observed region, a slit of length 145 arcsec, shown as a red rectangle. The teal lines denote the 1D spectrum extracted from the central 5 arcsec of the slit, corresponding to the central spectrum shown in Figure 2. The yellow lines denote the 1D spectrum extracted over the galaxy disc and is also shown in Figure 4. The scale bar shown in the top left corner corresponds to 10 arcsec.

2.1 AGN host Sample

In order to investigate SMBH growth in the merger-free regime, we require a sample of AGN hosted in disc-dominated galaxies with little–to–no bulge component. The sample used here was first compiled in Simmons et al. (2017), and we summarise the sample selection here.

The initial sample of AGN is selected using the W2R sample (Edelson & Malkan 2012), which were identified via a multi-wavelength approach using the Wide-Field Infrared Survey Explorer (WISE; Wright et al. 2010), Two Micron All-Sky Survey (2MASS; Skrutskie et al. 2006) and the ROSAT All-Sky Survey (RASS; Voges et al. 1999). This photometric, all-sky selection combines both infrared and X-Ray selection to identify 4,316 unobscured AGN. (Edelson & Malkan 2012). Simmons et al. (2017) use the Sloan Digital Sky Survey (SDSS; York et al. 2000) to select from the AGN sample a set of galaxies that are dominated by the presence of a disc. Using SDSS Data Release 8 (DR8; Aihara et al. 2011), there are 1,844 sources within 3 arcsec of a source in the W2R sample. A single expert classifier (BDS) used the SDSS colour images to perform a morphological selection, and found that there were 137 galaxies lacking visual evidence of a bulge component, but containing features commonly found in discs (spiral arms, bars etc.). Many of these galaxies have SDSS fibre spectra focused on the nuclei of each source. However, in order to reliably determine SFRs in these Type-1 AGN with very strong emission lines, we require off-nuclear spectra.

Longslit spectroscopic data was taken from the Kast Spectrograph on the Shane Telescope at Lick Observatory over 18 nights in the period 2016 October to 2018 November for 56 of these sources, in order to work towards spectroscopic completion of the parent sample. Despite the 18 nights on sky, we were unable to obtain full spectroscopic completion of the sample, and 4 of these 137 sources

is completed negates any issues that arise when identifying bars at different resolutions. After removing all inactive discs with $z >$ 0.187, we are left with our comparison parent sample of 26,899 galaxies, which we refer to below as INACDISCS.

2.3 Data Reduction and Fitting

2.3.1 Lick Data Reduction

We used the Image Reduction and Analysis Facility (IRAF; Tody 1986, 1993) to reduce the longslit AGNDISCS spectra, and its packages designed specifically for longslit data reduction, NOAO.TWODSPEC.LONGSLIT, and NOAO.TWODSPEC.APEXTRACT. The Kast spectrograph has a red CCD and a blue CCD, and these were reduced separately. The instrument settings for all runs were: dichroic d57; blue grating 600/4310, red grating 600/7500. The slit width ranged from 2–3 arcsec, with a wider slit used for nights with particularly poor seeing. The overscan regions were subtracted, and the images were bias-subtracted and flat-fielded. There were a number of images, particularly in the red side of the detector, which were contaminated with cosmic rays, and for spectra taken in October 2016, stray alpha particles from a slightly radioactive instrument component that was later replaced. These artefacts were removed, and the images were calibrated for wavelength, then stacked according to the object and position angle. The background noise was subtracted from each combined image, and the images were extinction corrected. Standard stars, from which data was taken regularly throughout the night, were used to calibrate the flux at each wavelength. The standard stars used were: BD332642, BD284211, BD262606, Feige 34, Feige 110, G191B2B, G193-74, G24-9, GD248, HD157881, HD183143, HD19445, HD84937, HZ4. We use these standard stars to determine the point spread function (PSF) of the sources observed at that time. Since the standard stars are point sources, but have a Gaussian flux profile when observed, we can take the PSF to be the full–width–half–maximum (FWHM) of the flux of the star when plotted as a 2D spectrum.

Using longslit spectra means we can extract spectra at many points across the observed region, and we do this to obtain a spectrum of the central AGN in each source as well as an off-nuclear spectrum of the galaxy. The required 1D spectra were extracted; the 5 pixels around the central AGN to form the AGN spectrum, and the galaxy from either 2σ or 3σ of the PSF out to the edge of the disc to form the galaxy spectrum. Following reduction and extraction, the blue and red CCD outputs were merged to give two full spectra per position angle per object – one of the galaxy and one of the AGN. Since the two sides of the detector each have a different spectral resolution, it is necessary to interpolate the region where the CCDs overlap. We aperture correct the AGN spectra to account for cases where the width of the slit is small compared to the PSF of the AGN. We assume that the central spectrum is dominated by AGN flux. This is due to our sample being selected so as to be the most luminous AGN. The slit and extraction regions are demonstrated in Figure 1 for galaxy J081324.00+542236.9. We show the resultant spectra of J081324.00+542236.9 in Figure 2, including an AGN spectrum, a galaxy spectrum and a variance spectrum.

2.3.2 Spectral Fitting

To fit the spectra, we used SCIPY (Virtanen et al. 2020), to fit a Gaussian function to each emission line along with a linear fit for the continuum emission near the line. The focus was on obtaining robust Hα and [O III] fits. For regions such as the Hα/[N II] complex, several

Gaussian functions were used to disentangle overlapping emission lines, as shown in Figure 3.

Where the signal–to–noise ratio was too low and we could not obtain accurate Hα fits of the sources, we determined the upper limit of Hα flux by assuming all the flux in the region where a detectable Hα emission line would have been is due to Hα, and integrating the spectrum in this range to give a conservative upper limit.

The spectra taken over the centre of the system differ greatly to those taken of the galaxy. This is due to the presence of the AGN, which can add considerable flux and cause broadening. Thus, for all the AGN spectra, we require an extra Gaussian component for Hα with a higher velocity dispersion than the corresponding narrow component. This broad Hα component was also present in some of the off-nuclear spectra, and so was included in the fitting process since the AGN contaminant requires fitting before its successful removal. The differences in the galaxy and AGN spectra can be seen in Figure 3, with the AGN spectrum shown in Figure 3a and the galaxy spectrum shown in Figure 3b.

Redshifts were calculated using spectral emission lines. We used the [O III] 5007Å emission line as the reference wavelength where possible, however if for reasons such as low signal–to–noise the [O III] 5007Å observed wavelength was unreliable, we used the Hα 6563Å emission line.
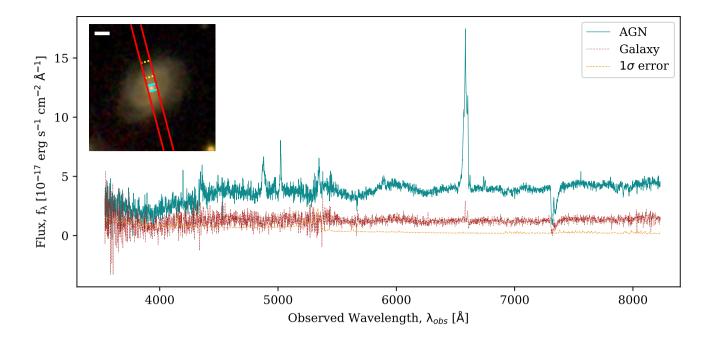
After fitting the galaxy spectra, the AGN contaminant was subtracted. We observe that the Shane/Kast PSF is Gaussian by examination of standard star spectra. Thus where we extracted the galaxy spectrum from 2σ away from the AGN to the edge of the disc, we subtract 2.5 per cent of the AGN emission from the galaxy emission (since it is only one side of the PSF in the slit). Where instead we start at 3σ, we subtract 0.015 per cent of the AGN emission. This gives us a final AGN host galaxy sample of 56 galaxies, 22 of which have upper limits constraining their Hα fluxes. This sample, which we refer to below as AGNDISCS, has median redshift $z_{med} = 0.0857$.
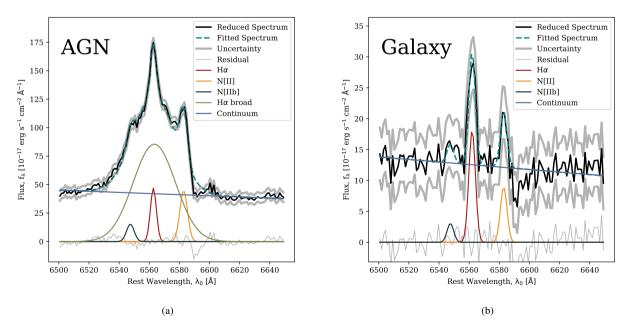
2.3.3 HST Data Reduction and Photometric Fitting

A subset of the AGN host galaxies selected via the method described above and analysed here were also observed with the *Hubble Space Telescope* (*HST*) Advanced Camera for Surveys (ACS) as part of a snapshot programme (HST-GO-14606, PI: B. Simmons). Given that it was a snapshot programme, we prioritised those galaxies whose morphology was less clear in SDSS photometry, in order that confident morphologies could be obtained for all of AGNDISCS as well as accurate decomposition of AGN and host galaxy, which we cover in more detail below. Each of the 43 systems in AGNDISCS with *HST* imaging was observed in a single broadband optical filter, chosen to minimise the contribution of bright AGN emission depending on the redshift of the source (i.e., to avoid either [O III] /Hβ or Hα; typically this choice resulted in selecting the *F*814*W* filter).

Each source was observed with 2 short exposures to ensure an unsaturated nuclear PSF, and 2 long exposures to reach an acceptable depth in the extended galaxy. A typical exposure time on source was approximately 40 minutes, with ACS/WFC subarrays chosen to minimise readout time whilst still imaging substantial sky background. The data was reduced using the standard reduction pipeline[1], including CCD charge diffusion correction and cosmic ray removal using LACosmic (van Dokkum 2001). The long exposures were combined
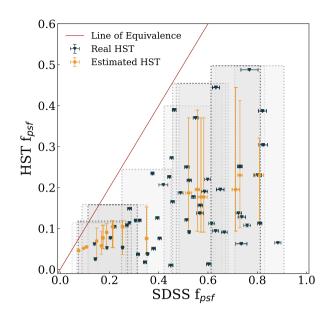
---

[1] At the time of data reduction, some manual steps were required as a result of using subarrays, but these configurations have since been incorporated into the standard imaging reduction pipeline.

Figure 2. Full example spectra of J081324.00+542236.9 with AGN (solid teal line) and galaxy spectra (dotted red line) shown, and variance in the galaxy spectrum (dashed orange line). The thumbnail in the top left corner shows the galaxy from which these spectra were taken, and the red lines on the thumbnail represent the part of the image observed by the slit. The spectrum shown in red dashes is the spectrum taken over the galaxy, excluding a significant amount of the flux from the AGN. This corresponds to the section of the slit enclosed in neon yellow dashed lines The spectrum shown in solid blue is the spectrum taken over the central five pixels of the source, which is dominated by the flux from the AGN. This corresponds to the section of the slit encased in solid neon blue. The Hα/[N ɪɪ] is easily detected in both spectra, with an additional broad Hα component in the AGN spectrum. The [O ɪɪɪ] and Hβ emission lines are not apparent in the galaxy spectrum, but can be clearly seen in the AGN spectrum.

Figure 3. Fitted spectra, with panel 3a showing the spectrum across the centre of the source including the AGN, and panel 3b showing the spectrum across the galaxy. The reduced spectrum is shown in black solid lines, and the fitted spectrum is shown in dashed turquoise, with the uncertainty in grey thick lines and the residual in grey thin lines. The components making up the fit are also shown, with the continuum in blue Hα in red, [N ɪɪ] in yellow, [N ɪɪb] in dark blue, and broad Hα in green (only present in the AGN spectrum). The AGN spectrum primarily differs from the galaxy spectrum by the addition of this broad Hα component.

Figure 4. The fraction of the flux contained within the PSF for both *HST* and SDSS, with the sources observed with *HST* in dark blue, and those for which we are lacking *HST* data shown in orange. In light grey, we show the bins from which $f_{\rm psf,HST}$ is estimated where we do not have *HST* data. We take a bin surrounding the $f_{\rm psf,SDSS}$ point, of width 0.2. Using the median $f_{\rm psf,HST}$ values from the points within that bin, we determine the equivalent $f_{\rm psf,HST}$. Thus there is one light grey bin for every source lacking *HST* data. The large error bars on the estimated $f_{\rm psf,HST}$ points are due to the large scatter. The fact that every point is either on or below the line of equivalence demonstrates that SDSS overestimates $f_{\rm psf}$, and hence we need *HST* data.

into a final science exposure. For the purposes of photometric fitting (described below), image fluxes of the reduced images are in counts.

The availability of *HST* imaging for part of AGNDISCS facilitates more accurate structural decomposition of these sources than was originally possible using SDSS images. The full details of AGN host structural decomposition of the *HST* images will be presented in a separate work (M. Fahey et al, in preparation). Briefly, we used the two-dimensional parametric image fitting program GALFIT (Peng et al. 2002, 2010) to simultaneously model the unresolved nucleus and extended galaxy for each of the sources in AGNDISCS that has *HST* imagery. Each image was background-subtracted, and the sky model fixed to zero. We constructed an empirical PSF in each band using background-subtracted images of isolated stars drawn from every observation in the *HST* snapshot programme described above.

We estimated initial guesses for fit parameters, using IRAF and SAOIMAGE DS9 (Joye & Mandel 2003) to measure central source positions and galaxy effective radii, as well as galaxy position angles and axis ratios. Each source was initially fit in an iterative 'batch' mode, starting with a single Sérsic (1968) profile for the galaxy model and a PSF for the AGN model. The host Sérsic index is set to $n = 2.5$ and allowed to vary. This value was chosen so as to avoid favouring either an exponential disc ($n = 1$) or a deVaucouleurs bulge ($n = 4$). Where present, we also fit and subtract nearby bright stars and extended companion galaxies, and mask fainter compact sources from the fit. Subsequent batch-fitting iterations of each source involve additional galaxy components, including a compact Sérsic component to model a potential pseudo- or classical bulge.

Following the completion of batch fitting, we followed up each

source to refine the fit. Where justified by inspection of fit residuals and reduced χ_ν^2, we refined the original fits and/or added additional components, including bars and spiral arms. In a few cases where the AGN emission saturated the detector in the long *HST* exposures, we determined the AGN-to-galaxy luminosity ratio using fits to the short-exposure images, fixing this AGN magnitude and masking out the saturated pixels in subsequent fits to the galaxy in the long-exposure images. The overall goal of the fits to each source was to neither over- nor under-subtract the galaxy's central region. In addition, great care was taken to ensure the chosen galaxy best fit contains physically realistic component parameters.

The final photometric fits were used to determine the fraction of the total flux of the source coming from the AGN, $f_{\rm psf}$. This was done by assuming that the PSF component measured from the *HST* images, $f_{\rm psf,HST}$, is wholly due to the AGN point source in the centre of the system. For systems where *HST* imagery is available, $f_{\rm psf}$ is then calculated by dividing the fitted PSF by the sum of fluxes from all components. Throughout this paper, when referring to the galaxy flux, this is the the total flux multiplied by $\left(1 - f_{\rm psf}\right)$.

As mentioned above, *HST* images are not available for the entire AGNDISCS sample, and thus those sources lacking *HST* data require us to estimate their individual values of $f_{\rm psf}$. All sources in AGNDISCS have an estimate of $f_{\rm psf}$ from SDSS. We calculate this value, $f_{\rm psf,SDSS}$, for all sources in AGNDISCS using the psfMag and cModelMag SDSS photometric values to determine the PSF and to-tal source flux, respectively. As discussed in Simmons et al. (2017), $f_{\rm psf,SDSS}$ is overestimated for these systems given their bright nu-clear emission and the resolution of SDSS compared to the size of the galaxies. Given that *HST* has a factor of ∼ 8 better resolution, we expect the *HST*-derived values of $f_{\rm psf}$ to be far more accurate. Figure 4 shows the values of $f_{\rm psf}$ from both SDSS and *HST* for each system with available *HST* images. The $f_{\rm psf,SDSS}$ is higher than $f_{\rm psf,HST}$ for *every* system, confirming the predictions of Simmons et al. (2017). Additionally, the 43 systems in AGNDISCS with mea-surements from both SDSS and *HST* allow us to determine a relation between the lower-resolution and higher-resolution measures, which we apply to the remaining systems without *HST* data. Specifically, we determine a running median of the ratio between *HST* and SDSS PSF flux fractions, using a sampling width of 0.2 in SDSS PSF flux fraction. We extrapolate this median, assuming a linear increase, for the 6 data points outside the range of values observed in the subset of AGNDISCS with both *HST* and SDSS measurements. For each source lacking an *HST* image, we assume the *HST* $f_{\rm psf}$ is equal to the SDSS PSF fraction times the median ratio, with an uncertainty determined by sampling the scatter in the distribution at that value. The estimated values of $f_{\rm psf}$ and their uncertainties are shown in Figure 4.

2.4 Bar presence

There are several methods used to classify bars, most commonly via ellipse fitting (e.g Regan & Elmegreen 1997), and visually (e.g. Nair & Abraham 2010). The method used is unlikely to affect final counts, as demonstrated in Sheth et al. (2008), who used both methods to classify their sample of over 2000 face-on, spiral galaxies into strongly barred, intermediate barred and non-barred. They found that the two methods agreed in 85 per cent of cases, and in a further 10 per cent of cases, only disagreed by one class. A further method of bar classification is using GZ2, which classifies a galaxy's bar status in the same style as the identification of discs (Section 2.2). Once a volunteer has established that the source is a disc that is not edge-on, they are asked "Is there a sign of a bar feature through the centre of

the galaxy?". GZ2 has been shown in multiple studies (e.g. Masters et al. 2011; Simmons et al. 2014) to robustly identify bars. Melvin et al. (2014) used Galaxy Zoo Hubble (GZH), which follows the same question tree as GZ2, to investigate bar fraction with redshift, and their results are in strong agreement with Sheth et al. (2008). This shows that the three methods – ellipse fitting, visual, and Galaxy Zoo – can all be used in conjunction with each other to obtain robust classifications of bar status. Many previous GZ2 bar studies focus on strong bars, and thus use a relatively high threshold for bar selection (e.g., $p_{bar} \geq 0.5$). Willett et al. (2013) show that the optimal GZ2 vote fraction for including both strong and weak bars in an analysis of population bar fractions is $p_{bar} \geq 0.3$.

For AGNDISCS, visual identification of a bar was performed by a single expert classifier (ILG) using the *HST* images for the 43 sources that have such data available. The same classifier then repeated this visual identification for the 23 sources for which we are lacking *HST* data using SDSS images of the galaxies. Only two galaxies in AGNDISCS had been classified in GZ2, thus we did not use GZ2 to identify bar presence. We note that due to the brightness of the AGN, we may have missed some smaller bars that would still be classed as galactic-scale, and acknowledge that this is an additional source of asymmetric uncertainty, and thus the true bar fraction for this sample may be higher than we show.

The bar status of all the galaxies in INACDISCS was determined using a GZ2 bar vote fraction threshold of $p_{bar} \geq 0.3$. A number of these were visually checked by ILG to ensure consistency with AGNDISCS. The results presented in Section 5 do not depend strongly on the vote fraction threshold.

2.5 Bulge Classification

We classify the galaxies in INACDISCS into those containing a bulge at the centre of their disc, and those that have a bulge prominence no greater than that in AGNDISCS, following the method outlined in Masters et al. (2019, Equation 3) to determine the bulge prominence, B_{avg} using GZ2. After deciding whether a disc galaxy has a bar, volunteers are asked 'How prominent is the central bulge, compared with the rest of the galaxy?' and presented with four options: 'No bulge', 'Just noticeable', 'Obvious', and 'Dominant'.

$$B_{avg} = 0.2p_{just\ noticeable} + 0.8p_{obvious} + 1.0p_{dominant} \tag{2}$$

By visually inspecting whether a subsample of galaxies are visually bulgeless, we determine what value of B_{avg} we require so that the bulge prominence parameter agrees with visual observations. A useful condition for a disc galaxy that is not edge-on to be classified as having a bulge prominence in line with AGNDISCS is $B_{avg} \leq 0.3$.

3 STELLAR PROPERTIES OF THE SAMPLES

Given that we need to control for SFR and stellar mass, M_*, we first need to measure these parameters, and we describe this process below. Figure 5 shows the SFR-M_* distribution of the parent inactive sample, INACDISCS (dark blue contours), and the complete disc-dominated, AGN host sample, AGNDISCS (red crosses). The two samples, whilst they have significant overlap in their distributions, occupy very different parameter spaces. The process for obtaining M_* is described in the Section 3.1, and the process for obtaining SFR is described in Section 3.2.

3.1 Stellar Mass

For the INACDISCS sample, we use the median stellar mass value reported in the MPA-JHU catalogue (Kauffmann et al. 2003a; Salim et al. 2007; Brinchmann et al. 2004) for each individual galaxy. This is possible since there are no bright AGN in the galaxies in INACDISCS, so there is no need to account for the flux coming from the AGN contaminating the galaxy flux. The minimum M_* is $\log(M_*) = 7.20$ and the maximum SFR is $\log(M_*) = 12.06$. The median is $\log(M_*) = 9.80$.

It is important that stellar mass is calculated in as similar way as possible for both samples. Kauffmann et al. (2003a) used SDSS-derived spectral indices to determine stellar masses, correcting for a number of potential biases, including for the size and partial galaxy coverage of the spectral fibre aperture. They also found a tight relation between galaxy colour and mass-to-light ratio. The colour-based M/L determination directly uses the integrated light of the whole galaxy. In addition to being generally useful for galaxies where no spectrum is available, this method is likely to be more robust to contamination from luminous AGN than the method based on fibre spectra.

We estimate M_* for the AGNDISCS sample using the colour-dependent mass-to-light ratio determinations of Baldry et al. (2006, Figure 5). This method requires $u - r$ colours for the host galaxies, disentangled from the bright AGN emission. We assume that our measured f_{psf} values (Section 2.3.3) are a better measure of AGN and host galaxy flux ratios than the SDSS psfMag in every band, and thus apply the factor of $(1 - f_{psf})$ to the u and r band cModelMag to determine galaxy u and r magnitudes. The minimum M_* is $\log(M_*) = 9.93$ and the maximum M_* is $\log(M_*) = 11.19$. The median is $\log(M_*) = 10.71$.

From Figure 4, we can see that had we used exclusively f_{psf} from SDSS, the values for M_* would tend to be underestimated, since the fraction of the total flux assigned to the AGN would be greater than the true value, leading to a lower flux being assigned to the galaxy. Following the equations in Baldry et al. (2006), this would lead to a lower M_*. Our improved PSF subtraction allows us to determine stellar masses for the AGN sample that more closely match the masses determined for the inactive sample. In Section 4 we also match the stellar mass distributions between AGNDISCS and INACDISCS.

3.2 Star Formation Rate

As with M_* it is important that the methods for calculating SFR in AGNDISCS and INACDISCS are as similar as possible, whilst acknowledging that only one sample has a source of flux of contamination in the form of an AGN.

We use the formula outlined in Kennicutt et al. (1994), succinctly expressed in solar units in Pflamm-Altenburg et al. (2007, Equation 14) to determine the SFR of individual galaxies in AGNDISCS, where $L_{H\alpha}$ is the Hα luminosity.

$$\frac{SFR}{M_\odot\ yr^{-1}} = \frac{L_{H\alpha}}{1.26 \times 10^{41}\ erg\ s^{-1}} \tag{3}$$

However, this only gives the SFR within the region observed with Lick (see Figure 1), SFR_{obs}, and requires extrapolation to the rest of the galaxy, SFR_{gal}. We do this via simplification of the method outlined in Brinchmann et al. (2004), which assumes that SFR directly correlates with the luminosity in the i-band. We determine the i-band luminosity in the observed region, $L_{i,obs}$, by convolving the spectrum with the i-band filter transmission curve (Rodrigo et al.

2012; Rodrigo & Solano 2020). We use the SDSS `cModelMag` from the MPA-JHU catalogue to calculate the i-band luminosity of the galaxy, $L_{i,gal}$ (via use of f_{psf}), and scale up the SFR accordingly via:

$$\text{SFR}_{\text{gal}} = \frac{L_{i,\text{gal}}}{L_{i,\text{obs}}} \text{SFR}_{\text{obs}} \qquad (4)$$

Using SDSS flux measurements from MPA-JHU, the inactive sample is consistent with a single value of 0.3 ± 0.1 for the Balmer decrement, assuming a gas temperature of $T = 10^4$ K, an electron density of $n_e = 10^2\,\text{cm}^{-2}$, Case B recombination (Osterbrock 1989), and a reddening curve defined in Calzetti et al. (2000). We assume that this also applies to the star-forming regions of the AGN-host galaxies, and thus apply this Balmer decrement as shown in Domínguez et al. (2013).

There are 22 sources in AGNDISCS for which we were unable to obtain values of Hα flux in the galaxy, and can only constrain the upper limit. This is due to no discernible signal, even after carefully removing the AGN contamination from the galaxy using the wings of the PSF, as described in Section 2.3.2. Thus, for galaxies that have an upper limit to their Hα flux, they only have an upper limit for their SFR.

Since the sources in INACDISCS do not host a bright AGN contaminating the emission from the galaxy, we can directly use the values in MPA-JHU for total SFR (as opposed to the SFR exclusively in the central fibre), given as `MEDIAN_SFR`, which also uses the method outlined in Brinchmann et al. (2004). The minimum SFR is $\log(\text{SFR}) = -2.40$ and the maximum SFR is $\log(\text{SFR}) = 1.93$. The median is $\log(\text{SFR}) = 0.026$.

3.2.1 Dealing with upper limits

We identify whether the 22 galaxies with no detected Hα emission are consistent within our S/N limits with being drawn from the subsample of 34 galaxies in AGNDISCS with Hα detections. We use a bootstrapping method to randomly sample from within the upper limits of the non-detected SFRs. Specifically, we assume the true values of SFR are uniformly distributed between the upper limit calculated, and a lower end of $\log(\text{SFR}) = -1.5$, where -1.5 was chosen as a small, non-zero number approximately equal to the lower end of SFRs in INACDISCS. A uniform distribution is a conservative estimate, since there is no reason to assume that the true value of the SFR is closer to the upper limit than to anywhere else in the range – we have no prior information about the distribution of SFRs. We also select a random sample from the sources with Hα detections, where the SFR was randomly drawn from a normal distribution with a mean of $\log(\text{SFR})$ and a standard deviation of the error in $\log(\text{SFR})$. We re-sampled from upper limit SFRs and values of SFR using this method 100,000 times, with replacement. For each sampling, we used a KS test (Kolmogorov 1933) to identify the probability that the two samples were drawn from the same distribution. If the SFRs of the limited subsample are statistically indistinguishable from those in the measured subsample, we would expect the KS values to follow a Normal distribution. For example, we would expect approximately 95 per cent of tests to have $p > 0.05$.

Instead, the distribution of KS values from the bootstrapping is highly skewed toward more statistically significant differences. Only 0.077 per cent of the selections and comparisons had $p > 0.05$. In other words, a $> 2\sigma$ confidence that the two samples were statistically indistinguishable only occurred 77 times out of 100,000. If the subsample with limits was indistinguishable from that without, we would expect this to occur approximately 95,000 times. Therefore

Figure 5. SFR against M_*, for both the active sample, AGNDISCS (red crosses) and the inactive disc-dominated sample, INACDISCS (dark blue contours). Upper limits for SFR in the active sample are shown as arrows and in a slighter paler red than those with values. Normalised histograms are shown on the top and right axes, with the thick red line corresponding to AGNDISCS and the thin blue line to INACDISCS.

the sources with SFR limits do have significantly lower SFRs than the rest of the sample, but our inability to otherwise constrain them inhibits a clean comparison with the inactive sample. Thus, for comparisons using a tightly controlled sample, we remove the sources which have only upper limits on their SFR, instead of Hα detections.

This gives us an AGN host galaxy sample used for comparison, which we call AGNDISCFIN, of median redshift 0.13, containing 34 galaxies, 20 of which host a large-scale galactic bar. The fraction of this sample hosting a bar is $f_{\text{bar,AGN}} = 0.59^{+0.08}_{-0.09}$, where uncertainties enclose the 68 per cent confidence limits of the binomial fraction error (Cameron 2011). The minimum SFR is $\log(\text{SFR}) = -1.16$ and the maximum SFR is $\log(\text{SFR}) = 2.08$. The median is $\log(\text{SFR}) = 0.56$.

With both M_* and SFR derived from AGN-subtracted galaxy fluxes, we can examine further the star-forming properties of the sample below.

4 STAR FORMATION IN MERGER-FREE AGN HOSTS

In order to examine SFRs in both the AGN host and inactive galaxy samples, we must first control for differences in stellar mass. Figure 5 shows that whilst there is considerable overlap in the two samples in their stellar mass distributions, the distributions remain noticeably different – for active galaxies the distribution is narrower than for inactive galaxies, with the average active galaxy's M_* lying above the median M_* of inactive galaxies. This pattern remains upon the removal of the galaxies with only upper limits on their star formation rate.

The difference in M_* between the two samples is most likely due to selection effects rather than an intrinsic difference. AGNDISCS is selected as a sample to host only the most luminous AGN. If we

assume that the sample is not as a whole exceeding the Eddington limit, this means that there is a lower limit on black hole mass, M_{BH}. It is broadly understood that there is some form of co-evolution between galaxies and SMBHs (e.g. Kormendy & Ho 2013), even if we continue as a field to debate the details. Thus a lower limit on M_{BH} implies a lower limit on M_*, and the sample is therefore self-limiting regarding M_* (for a deeper exploration of this selection bias, see Aird et al. 2012).

The other way that AGNDiscs self-limits in M_* is that the sample is selected to consist of strongly disc-dominated galaxies. The galaxies were identified using SDSS, where the PSF width may be a substantial fraction of a galaxy's extent. If a low-mass disc-dominated galaxy hosted a very luminous AGN, the AGN would outshine the galaxy and the disc would be difficult or impossible to identify in SDSS imagery at the redshifts of this sample. Such a galaxy would not be included in AGNDiscs. Therefore there is a lower limit on disc radius, which implies a lower limit on M_*.

These two selection effects mean we have very few AGN hosted in galaxies with $M_* < 10^{10} \, M_\odot$ in our sample, and hence we must select galaxies from InacDiscs which have the same M_* distribution before comparing SFRs between the samples.

We control for M_* by weighting the inactive sample in six bins of equal width. This M_*-matched subset of inactive disc galaxies is hereafter called the InacDiscMatch sample, and its M_* distribution is shown in Figure 6a, for comparison with AGNDiscFin. After performing a KS test on AGNDiscFin's and InacDiscs's M_* to confirm their similarity, we obtain a p-value of $p_{mass} = 1.000$, which demonstrates that AGNDiscFin and InacDiscMatch are consistent with being drawn from the same parent sample.[2] The distribution of SFRs for the M_*-matched AGNDiscFin and InacDiscMatch samples are shown in Figure 6b. The slight visual differences between the distributions do not appear to be statistically significant (KS $p_{SFR} = 0.368$, a significance of 0.9σ). Thus we cannot rule out the null hypothesis that the SFRs of these disc-dominated galaxies hosting luminous Type-1 AGN are drawn from the same parent population as a sample of disc-dominated galaxies *not* hosting AGN. Our qualitative results do not change if we instead draw M_*-matched sub-samples instead of weighting the respective distributions.

While a lack of statistically significant differences in the SFRs of these subsamples may be due to our relatively small sample sizes, we might expect such a result even with a larger sample, due to the complex physical processes at play. For example, AGN outflows may both quench and enhance star formation in a host galaxy (see Harrison 2017 for a review). A high fraction of our AGN host sample shows signs of outflows (Smethurst et al. 2019, 2021), and these galaxies do not congregate in a specific region of SFR–M_* space (Figure 5), consistent with expectations. Differing timescales also complicate interpretation of our results: the duration over which an AGN is active in a galaxy may be considerably shorter than the effects of AGN-driven quenching (Schawinski et al. 2015), which would further dilute differences between SFR in the AGN host and inactive disc galaxy population. Better constraints on population differences between disc-dominated AGN host and inactive galaxies will require a larger sample, ideally with spatially-resolved spectral information to more robustly trace the effect of AGN feedback.

[2] All reported p-values for KS tests between weighted distributions are estimated using sample weights instead of raw object counts.

Table 1. KS test p-values from the comparisons described in Sections 4 and 5. These values are all indicative of statistically indistinguishable samples. Bold values indicate where we intentionally control for the samples to be statistically indistinguishable.

Samples being compared	p_{mass}	p_{SFR}
Controlling only for stellar mass		
AGNDiscFin (34), InacDiscMatch (34)	**1.000**	0.368
AGN Bar (20), AGN Non-bar (14)	0.814	0.648
Inac Bar (15), Inac Non-bar (19)	1.000	1.000
AGN Bar (20), Inac Bar (15)	1.000	0.554
AGN Non-bar (14), Inac Non-bar (19)	1.000	0.710
Controlling for stellar mass and SFR		
AGNDiscFin (34), InacDiscMatch (34)	**1.000**	**1.000**
AGN Bar (20), AGN Non-bar (14)	0.814	0.648
Inac Bar (15), Inac Non-bar (19)	1.000	0.977
AGN Bar (20), Inac Bar (15)	1.000	0.984
AGN Non-bar (14), Inac Non-bar (19)	0.999	0.955

5 BAR FRACTIONS OF AGN HOST VS INACTIVE DISCS

In order to isolate the possible effect of large-scale, galactic bars, we first need to ensure that all other variables which are known to correlate with bar fraction are negated via careful weighting in M_* and SFR to obtain a comparison sample. We use the star-forming sequence shown in Figure 5 to ensure that both the active and inactive samples are consistent with each other in their M_* and SFR, an additional control compared to Section 4, where we only control for M_*. As with M_*, there is significant overlap in SFR between the two samples. Whilst the SFR for active galaxies seems to cover approximately the same range as that for inactive galaxies, when we only control for M_* the samples still differ enough in SFR that we need to control for SFR in order to analyse the bar fraction. The medians of the two samples are $SFR_{AGN} = 0.59$ and $SFR_{inactive} = 0.72$, and the ranges are $-1.16 \leq SFR_{AGN} \leq 2.18$ and $-0.62 \leq SFR_{inactive} \leq 1.69$. Given that the two samples have different distributions, it is vital that we control for SFR as well as M_*, in order to truly isolate the effect of the bar.

We divide the M_* and SFR each into six bins, and assign weights to each galaxy in InacDiscs, such that the weighted sample (which we hereafter call InacDiscMatch) has M_* and SFR distributions matching those of AGNDiscFin. This gives a weighted bar fraction for InacDiscMatch of $f_{bar,Inac} = 0.44^{+0.08}_{-0.09}$, where uncertainties arise from the binomial fraction error (Cameron 2011).

We show the distributions of the control samples, split by active/inactive and by barred/non-barred, with M_* in Figure 7a, and SFR in Figure 7b. As expected, the distributions cover a much more similar range than in Figure 5. We confirm via KS tests on AGNDiscFin and InacDiscMatch that their M_* and SFR distributions are consistent with being drawn from the same parent sample.

We also use KS tests to compare both the SFR and the M_* for different subsets of the comparison samples – active galaxies, inactive galaxies, barred galaxies and non-barred galaxies. Table 1 shows the p-values that result from the comparison samples in the first column. Values for the inactive subsamples are the weighted numbers.

Looking at the bar fractions ($f_{bar,AGN} = 0.59^{+0.08}_{-0.09}$ for AGNDiscFin and $f_{bar,Inac} = 0.44^{+0.08}_{-0.09}$ for InacDiscMatch), we can see that after controlling for the SFR and M_*, the sources in InacDiscMatch are marginally less likely ($\sim 1.7\sigma$) to host a bar than the sources in AGNDiscFin, in agreement with studies such as Alonso et al. (2013)
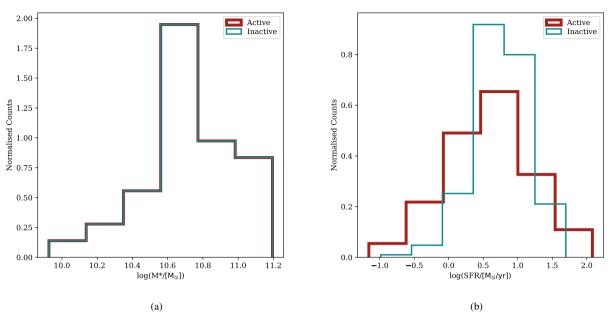
Figure 6. Distribution of M_* (left panel) and SFR (right panel) after controlling for M_*, with AGN host galaxies shown in thick red lines and inactive galaxies shown in thin blue lines. The M_* distribution demonstrates that we have successfully controlled for M_*, and has a p-value from a KS test of 1.000, showing the samples are consistent with being drawn from the same parent sample. The SFR histogram also shows the similarity between the two samples after controlling for M_*, and with a p-value of 0.368, the SFR's are consistent with being drawn from the same parent sample.

and Galloway et al. (2015). However it is worth noting that the samples used by Galloway et al. (2015) contain $\sim 10^5$ galaxies and this work contains $\sim 10^2$ galaxies, yet both studies obtain a similar level of significance in their results. This could potentially be due to the fact that we are looking at galaxies with little–to–no bulge component, so any bars we have are likely to be younger than in Galloway et al. (2015) where they make no distinction on bulge component, and thus we do not require such a large sample to obtain a similarly significant result. Our sample also considers only the highest luminosity AGN, whereas again, Galloway et al. (2015) impose no such limit on their sample.

We can use the p-values from the KS tests shown in the second section of Table 1 to rule out the null hypothesis that two samples are drawn from the same parent distribution. The first line, comparing AGNDISCFIN to INACDISCMATCH before controlling for SFR shows that overall the comparison samples are consistent with being drawn from the same parent sample. This is a simple check to confirm we have controlled for the various parameters correctly. From here, we divide each sample into barred and non-barred subsamples in order to draw comparisons.

For any M_*- and SFR-matched sub-samples we examine, we cannot rule out the null hypothesis that the two samples are drawn from the same parent distribution. Several potential insights emerge from this overall result. Firstly, within our samples, a bar does not necessarily have to be present to form an AGN, but if there is a bar there, then it has no unique further effect on the SFR and M_*. Secondly, the bar has no effect on SFR or M_* in this SFR–M_* regime. Lastly, barred AGN host galaxies are not a special subset of inactive barred galaxies, and this is mirrored by the comparison of active non-barred galaxies versus inactive non-barred galaxies, which also has p-values of SFR and M_* close to 1, i.e., far short of any reasonable threshold for statistically significant differences. This is much the same as results from works in the last few decades (e.g. Ho et al. 1997;

Mulchaey & Regan 1997; Knapen et al. 2000; Martini et al. 2003). We would note that our results do not qualitatively change if instead we only consider strong bars in both samples (i.e., excluding weak bars in the AGN host sample and using a threshold of $p_{bar} \geq 0.5$ for the inactive sample to select strong bars, as described in Section 2.4).

It is worth noting that whilst these results indicate solutions, our sample of AGN hosts being used to quantitatively compare is simply too small to draw conclusions with much statistical power. This is because these are the very brightest AGN in the most unambiguously disc-dominated host galaxies, rather than a sample taken over the entire AGN population in all merger-free hosts. A significant portion of our sample has only upper limits on their SFR, further constraining the sample size. Our analysis of those limits (Section 3.2.1) hints that higher signal–to–noise spectra permitting robust measurements of this subsample could provide further insight into our current results. Integral field spectroscopy for a large fraction of our sample would enable us to probe these galaxies in further detail, as would increasing the sample size by adding Vera Rubin Observatory's LSST survey (Ivezić et al. 2019), or getting more galaxies with Euclid or Roman. Since we are looking at a rare phenomenon (luminous AGN), in a rare subset of galaxies (bulgeless or nearly so), it really is important that we have a large volume so as to control for confounding variables and achieve statistically robust sample numbers. It is also crucial to remember that not all AGN are this luminous, this is a particular subset of AGN, and it was collected in such a way so as to show the possibilities of extreme conditions, and further data on less luminous AGN is needed to draw conclusions over the entire population.
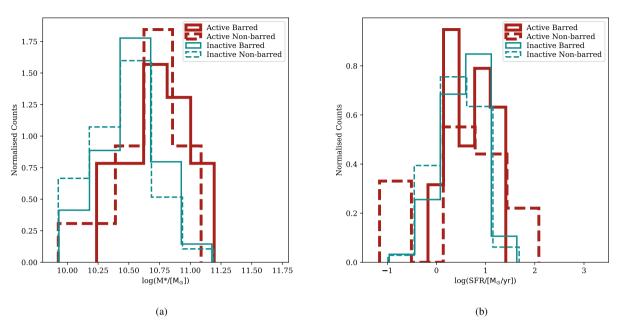
Figure 7. Distributions of M_* (left panel) and SFR (right panel), after controlling for both of these parameters, split by active (red, thick line) and inactive (thin blue line) galaxies, and by barred (solid line) and non-barred (dashed) lines. The results of KS tests between each pair of samples are shown in Table 1, but all the samples are consistent with being drawn from the same parent sample in both M_* and SFR.

6 CONCLUSIONS

We have used a sample of unambiguously disc-dominated galaxies hosting luminous, Type-1 AGN in order to isolate SMBH growth through merger-free processes. We obtained longslit Lick spectroscopic data of the sample, and *HST* images of part of the sample. This allowed us to measure robust SFRs and stellar masses for 34 galaxies – the rest of the sample has only upper limits on their SFR. We compared this sample to a sample of inactive, disc-dominated galaxies with morphological classifications from Galaxy Zoo 2, and SFRs and M_* from MPA–JHU. We performed KS tests on subsets of these samples, and we here summarise our findings:

- Galaxies hosting an AGN have a wider range of SFR than galaxies lacking an AGN, with the SFR peaking at a slightly higher value.
- After controlling for SFR and M_*, bars are marginally more likely to reside in AGN host galaxies than galaxies not hosting AGN, ($f_{\rm bar} = 0.59^{+0.08}_{-0.09}$ for AGNDISCFIN and $f_{\rm bar} = 0.44^{+0.08}_{-0.09}$ for INACDISCMATCH) – there is a $\sim 1.7\sigma$ difference.
- Despite the fact that bars are more likely to reside in massive galaxies, and AGN are more likely to reside in massive galaxies, having both a bar and an AGN is not associated with a further increase in a galaxy's stellar mass beyond only having one of either a bar or an AGN.

Further work is needed to obtain higher resolution spectra for those galaxies where the flux from the disc is so overpowered by the flux of the AGN that we can only obtain upper limits of their SFR. This will allow for better separation of the AGN and the galaxy, which will result in a higher signal–to–noise ratio, and allow us to constrain SFRs further.

Upcoming surveys such as LSST and Euclid will facilitate breakthroughs in the field due to their increased resolution and sky coverage, which will allow us to obtain larger samples of merger-free AGN host galaxies for improved statistical analysis. With today's facilities

and scientific ability, it is interesting to see that despite probing the extremes of black hole growth in the merger-free regime, for those galaxies where we can obtain SFR, they do not appear to be outliers compared to galaxies not hosting AGN.

Software

This research has made use of Topcat (Taylor 2005), an interactive graphical tool for analysis and manipulation of tabular data.

This research has made extensive use of the following Python packages:

- Astropy, a community-developed core Python package for Astronomy (Astropy Collaboration et al. 2013, 2018).
- Matplotlib, a 2D graphics package for Python (Hunter 2007).
- Numpy (Harris et al. 2020), a package for scientific computing.
- Scipy (Virtanen et al. 2020), a package for fundamental algorithms in scientific computing.

This research has made use of Iraf (Tody 1986, 1993) and its packages for longslit data reduction.

This research has made use of Galfit Peng et al. (2002, 2010) for fitting photometric data.

DATA AVAILABILITY

The data for AgnDiscs is available on request.

REFERENCES

Aihara H., et al., 2011, ApJS, 193, 29
Aird J., et al., 2012, ApJ, 746, 90
Aird J., Coil A. L., Georgakakis A., 2019, MNRAS, 484, 4360
Alonso M. S., Coldwell G., Lambas D. G., 2013, A&A, 549, A141
Ann H. B., Thakur P., 2005, ApJ, 620, 197
Astropy Collaboration et al., 2013, A&A, 558, A33
Astropy Collaboration et al., 2018, AJ, 156, 123
Athanassoula E., 1992, MNRAS, 259, 345
Athanassoula E., 2003, MNRAS, 341, 1179
Baldry I. K., Balogh M. L., Bower R. G., Glazebrook K., Nichol R. C., Bamford S. P., Budavari T., 2006, MNRAS, 373, 469
Barazza F. D., Jogee S., Marinova I., 2008, ApJ, 675, 1194
Bizzocchi L., et al., 2014, ApJ, 782, 22

Brinchmann J., Charlot S., White S. D. M., Tremonti C., Kauffmann G., Heckman T., Brinkmann J., 2004, MNRAS, 351, 1151
Calzetti D., Armus L., Bohlin R. C., Kinney A. L., Koornneef J., Storchi-Bergmann T., 2000, ApJ, 533, 682
Cameron E., 2011, Publ. Astron. Soc. Australia, 28, 128
Cheung E., et al., 2013, ApJ, 779, 162
Cheung E., et al., 2015, MNRAS, 447, 506
Ciotti L., Ostriker J. P., Proga D., 2010, ApJ, 717, 708
Cisternas M., et al., 2011, ApJ, 741, L11
Combes F., 2009, in Jogee S., Marinova I., Hao L., Blanc G. A., eds, Astronomical Society of the Pacific Conference Series Vol. 419, Galaxy Evolution: Emerging Insights and Future Challenges. p. 31 (arXiv:0901.0178)
D'Onghia E., Vogelsberger M., Hernquist L., 2013, ApJ, 766, 34
Davies R. I., Maciejewski W., Hicks E. K. S., Tacconi L. J., Genzel R., Engel H., 2009, ApJ, 702, 114
Domínguez A., et al., 2013, ApJ, 763, 145
Donner K. J., Thomasson M., 1994, A&A, 290, 785
Edelson R., Malkan M., 2012, ApJ, 751, 52
Erwin P., 2018, MNRAS, 474, 5372
Eskridge P. B., et al., 2000, AJ, 119, 536
Fabian A., 2012, ARA&A, 50, 455
Friedli D., Benz W., 1993, A&A, 268, 65
Galloway M. A., et al., 2015, MNRAS, 448, 3442
Géron T., Smethurst R. J., Lintott C., Kruk S., Masters K. L., Simmons B., Stark D. V., 2021, MNRAS, 507, 4389
Goulding A. D., et al., 2017, ApJ, 843, 135
Greene J. E., et al., 2010, ApJ, 721, 26
Häring N., Rix H.-W., 2004, ApJ, 604, L89
Harris C. R., et al., 2020, Nature, 585, 357
Harrison C. M., 2017, Nature Astronomy, 1, 0165
Hawarden T. G., Mountain C. M., Leggett S. K., Puxley P. J., 1986, MNRAS, 221, 41P
Hinshaw G., et al., 2013, ApJS, 208, 19
Ho L. C., Filippenko A. V., Sargent W. L. W., 1997, ApJ, 487, 591
Hunt J. A. S., Hong J., Bovy J., Kawata D., Grand R. J. J., 2018, MNRAS, 481, 3794
Hunter J. D., 2007, Computing in Science and Engineering, 9, 90
Ishibashi W., Fabian A. C., 2012, MNRAS, 427, 2998
Ivezić Ž., et al., 2019, ApJ, 873, 111
Jiang Y.-F., Greene J. E., Ho L. C., Xiao T., Barth A. J., 2011, ApJ, 742, 68
Joye W. A., Mandel E., 2003, in Payne H. E., Jedrzejewski R. I., Hook R. N., eds, Astronomical Society of the Pacific Conference Series Vol. 295, Astronomical Data Analysis Software and Systems XII. p. 489
Kauffmann G., et al., 2003a, MNRAS, 341, 33
Kauffmann G., et al., 2003b, MNRAS, 346, 1055
Kennicutt Robert C. J., Tamblyn P., Congdon C. E., 1994, ApJ, 435, 22
Kereš D., Katz N., Weinberg D. H., Davé R., 2005, MNRAS, 363, 2
Knapen J. H., Beckman J. E., Heller C. H., Shlosman I., de Jong R. S., 1995, ApJ, 454, 623
Knapen J. H., Shlosman I., Peletier R. F., 2000, ApJ, 529, 93
Kocevski D. D., et al., 2012, ApJ, 744, 148
Kolmogorov A., 1933, Inst. Ital. Attuari, Giorn., 4, 83
Kormendy J., Ho L. C., 2013, ARA&A, 51, 511
Kraljic K., Bournaud F., Martig M., 2012, ApJ, 757, 60
Kruk S. J., et al., 2018, MNRAS, 473, 4731
Laine S., Shlosman I., Knapen J. H., Peletier R. F., 2002, ApJ, 567, 97
Laurikainen E., Salo H., Buta R., 2004, ApJ, 607, 103
Lee G.-H., Woo J.-H., Lee M. G., Hwang H. S., Lee J. C., Sohn J., Lee J. H., 2012, ApJ, 750, 141
Lin L.-H., Wang H.-H., Hsieh P.-Y., Taam R. E., Yang C.-C., Yen D. C. C., 2013, ApJ, 771, 8
Maciejewski W., 2004, MNRAS, 354, 892
Maciejewski W., Teuben P. J., Sparke L. S., Stone J. M., 2002, MNRAS, 329, 502
Martig M., Bournaud F., Croton D. J., Dekel A., Teyssier R., 2012, ApJ, 756, 26
Martin G., et al., 2018, MNRAS, 476, 2801

Martini P., Regan M. W., Mulchaey J. S., Pogge R. W., 2003, ApJ, 589, 774
Masters K. L., et al., 2011, MNRAS, 411, 2026
Masters K. L., et al., 2012, MNRAS, 424, 2180
Masters K. L., et al., 2019, MNRAS, 487, 1808
McAlpine S., Harrison C. M., Rosario D. J., Alexander D. M., Ellison S. L., Johansson P. H., Patton D. R., 2020, MNRAS, 494, 5713
Melvin T., et al., 2014, MNRAS, 438, 2882
Miller R. H., Smith B. F., 1979, ApJ, 227, 785
Mulcahey C. R., et al., 2022, arXiv e-prints, p. arXiv:2206.01195
Mulchaey J. S., Regan M. W., 1997, ApJ, 482, L135
Mullaney J. R., et al., 2012, ApJ, 753, L30
Nair P. B., Abraham R. G., 2010, ApJS, 186, 427
Oh K., Sarzi M., Schawinski K., Yi S. K., 2011, ApJS, 195, 13
Oh S., Oh K., Yi S. K., 2012, ApJS, 198, 4
Osterbrock D. E., 1989, Astrophysics of gaseous nebulae and active galactic nuclei. University Science Books
Peng C. Y., Ho L. C., Impey C. D., Rix H.-W., 2002, AJ, 124, 266
Peng C. Y., Ho L. C., Impey C. D., Rix H.-W., 2010, AJ, 139, 2097
Pflamm-Altenburg J., Weidner C., Kroupa P., 2007, ApJ, 671, 1550
Regan M. W., Elmegreen D. M., 1997, AJ, 114, 965
Regan M. W., Teuben P. J., 2004, ApJ, 600, 595
Rodrigo C., Solano E., 2020, in XIV.0 Scientific Meeting (virtual) of the Spanish Astronomical Society. p. 182
Rodrigo C., Solano E., Bayo A., 2012, SVO Filter Profile Service Version 1.0, IVOA Working Draft 15 October 2012, doi:10.5479/ADS/bib/2012ivoa.rept.1015R
Sakamoto K., Okumura S. K., Ishizuki S., Scoville N. Z., 1999, ApJ, 525, 691
Salim S., et al., 2007, ApJS, 173, 267
Sancisi R., Fraternali F., Oosterloo T., van der Hulst T., 2008, A&ARv, 15, 189
Satyapal S., Böker T., Mcalpine W., Gliozzi M., Abel N. P., Heckman T., 2009, ApJ, 704, 439
Satyapal S., et al., 2016, ApJ, 827, 58
Schawinski K., Treister E., Urry C. M., Cardamone C. N., Simmons B., Yi S. K., 2011, ApJ, 727, L31
Schawinski K., Koss M., Berney S., Sartori L. F., 2015, MNRAS, 451, 2517
Schaye J., et al., 2015, MNRAS, 446, 521
Schnorr-Müller A., Storchi-Bergmann T., Nagar N. M., Ferrari F., 2014, MNRAS, 438, 3322
Sellwood J. A., 2014, Reviews of Modern Physics, 86, 1
Sérsic J. L., 1968, Atlas de Galaxias Australes. Observatorio Astrònomico
Sheth K., et al., 2008, ApJ, 675, 1141
Shlosman I., Frank J., Begelman M. C., 1989, Nature, 338, 45
Shlosman I., Begelman M. C., Frank J., 1990, Nature, 345, 679
Silverman J. D., et al., 2009, ApJ, 696, 396
Simmons B. D., Van Duyne J., Urry C. M., Treister E., Koekemoer A. M., Grogin N. A., GOODS Team 2011, ApJ, 734, 121
Simmons B. D., Urry C. M., Schawinski K., Cardamone C., Glikman E., 2012, ApJ, 761, 75
Simmons B. D., et al., 2013, MNRAS, 429, 2199
Simmons B. D., et al., 2014, MNRAS, 445, 3466
Simmons B. D., Smethurst R. J., Lintott C., 2017, MNRAS, 470, 1559
Skibba R. A., et al., 2012, MNRAS, 423, 1485
Skrutskie M. F., et al., 2006, AJ, 131, 1163
Smethurst R. J., Simmons B. D., Lintott C. J., Shanahan J., 2019, MNRAS, 489, 4016
Smethurst R. J., et al., 2021, MNRAS, 507, 3985
Sparke L. S., Sellwood J. A., 1987, MNRAS, 225, 653
Taylor M. B., 2005, in Shopbell P., Britton M., Ebert R., eds, Astronomical Society of the Pacific Conference Series Vol. 347, Astronomical Data Analysis Software and Systems XIV. p. 29
Tody D., 1986, in Crawford D. L., ed., Society of Photo-Optical Instrumentation Engineers (SPIE) Conference Series Vol. 627, Instrumentation in astronomy VI. p. 733, doi:10.1117/12.968154
Tody D., 1993, in Hanisch R. J., Brissenden R. J. V., Barnes J., eds, Astronomical Society of the Pacific Conference Series Vol. 52, Astronomical Data Analysis Software and Systems II. p. 173
Virtanen P., et al., 2020, Nature Methods, 17, 261
Voges W., et al., 1999, A&A, 349, 389
Willett K. W., et al., 2013, MNRAS, 435, 2835
Wright E. L., et al., 2010, AJ, 140, 1868
York D. G., et al., 2000, AJ, 120, 1579
van Dokkum P. G., 2001, PASP, 113, 1420

APPENDIX A: SDSS THUMBNAILS

Figure A1 shows the full AGNDiscs sample imaged in SDSS, with the scale bar in each image representing 10 arcsec. The disc-dominated nature of the galaxies can be seen clearly, as well as a large-scale galactic bar in some images.

APPENDIX B: *HST* THUMBNAILS

Figure B1 shows the galaxies for which we have *HST* data. Their position in the grid corresponds to their SDSS counterpart in Figure A1, however their rotation does not. The scale bar in these images corresponds to 5 arcsec. The grey blank squares show galaxies for which we do not have *HST* photometric data.

This paper has been typeset from a TEX/LATEX file prepared by the author.

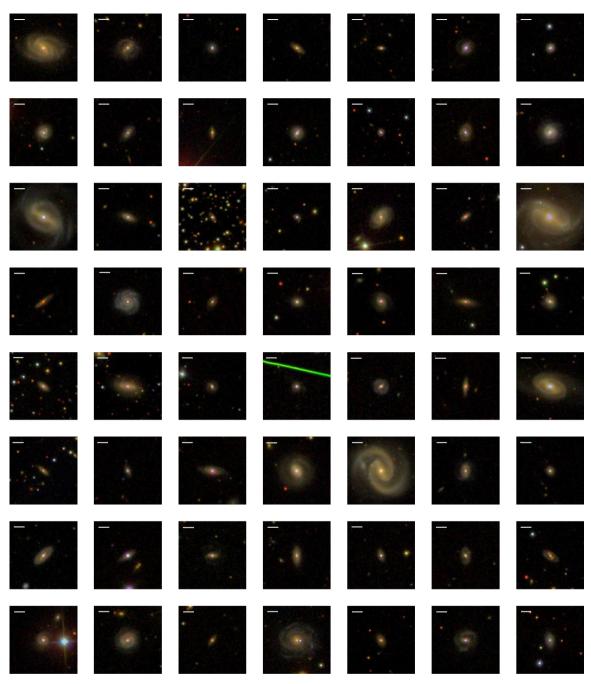**Figure A1.** SDSS postage stamps of all galaxies in AɢɴDɪsᴄs, including those that are constrained only by an upper limit in Hα, and those with values. Images are taken from SDSS DR8 (Aihara et al. 2011). The scale bar in each upper left corner represents 10 arcsec. The position angles of the galaxies do not correspond to those in Figure B1.
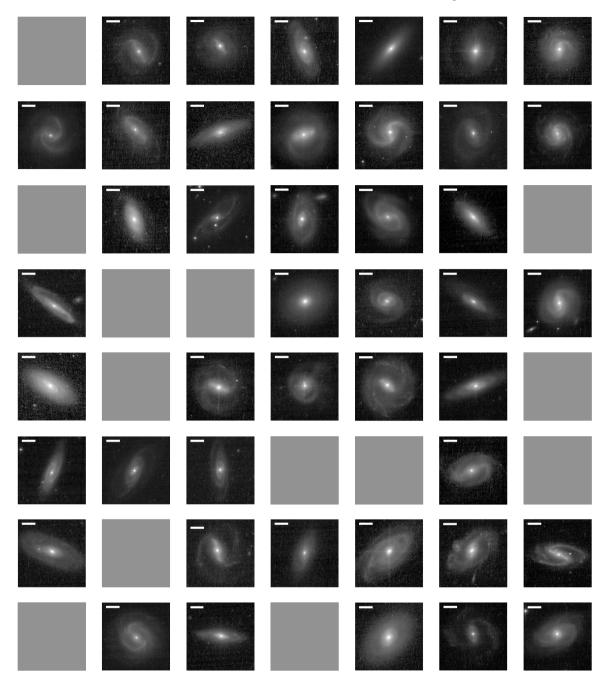
Figure B1. *HST* postage stamps of the galaxies in AɢɴDɪꜱᴄꜱ that have been imaged in *HST*. The galaxies' positions correspond to the galaxies in Figure A1, and so the grey squares represent galaxies that have not yet been imaged with *HST*. The white scale bar in each top left corner represents 5 arcsec. The position angles of the galaxies do not correspond to those in Figure A1.